Appl Phys A (2011) 104:109–116
DOI 10.1007/s00339-011-6294-3

Applied Physics A
Materials Science & Processing

Effects of La–Zn substitution on microstructure and magnetic properties of strontium ferrite nanofibers

Xiangqian Shen · Mingquan Liu · Fuzhan Song · Yongwei Zhu

Received: 28 June 2010 / Accepted: 10 January 2011 / Published online: 26 January 2011

Abstract $Sr_{1-x}La_xZn_xFe_{12-x}O_{19}$/poly(vinylpyrrolidone) (PVP) ($0.0 \leq x \leq 0.5$) precursor nanofibers were prepared by the sol–gel assisted electrospinning method from starting reagents of metal salts and PVP. Subsequently, the $Sr_{1-x}La_xZn_xFe_{12-x}O_{19}$ nanofibers with diameters of around 100 nm were obtained by calcination of the precursor at 800 to 1000°C for 2 h. The precursor and resultant $Sr_{1-x}La_xZn_xFe_{12-x}O_{19}$ nanofibers were characterized by X-ray diffraction, scanning electron microscopy, energy-dispersive X-ray spectrometer and vibrating sample magnetometer. The grain sizes of $Sr_{0.8}La_{0.2}Zn_{0.2}Fe_{11.8}O_{19}$ nanofibers are in a nanoscale from 40 to 48 nm corresponding to the calcination temperature from 800 to 1000°C. With La–Zn substitution content increase from 0 to 0.5, the grain size and lattice constants for the $Sr_{1-x}La_xZn_xFe_{12-x}O_{19}$ nanofibers obtained at 900°C show a steady reduction trend. With variations of the ferrite particle size arising from the La–Zn substitution, the nanofiber morphology changes from the necklace-like structure linking by single elongated plate-like particles to the structure building of multi-particles on the nanofiber cross-section. The specific saturation magnetization of $Sr_{1-x}La_xZn_xFe_{12-x}O_{19}$ nanofibers initially increases with the La–Zn content, reaching a maximum value $72\,A\,m^2\,kg^{-1}$ at $x = 0.2$, and then decreases with a further La–Zn content increase up to $x = 0.5$, while the coercivity exhibits a continuous reduction from 413 ($x = 0$) to $219\,kA\,m^{-1}$ ($x = 0.5$). The mechanism for the La–Zn substitution and the nanofiber magnetic property are analyzed.

X. Shen (✉) · M. Liu · F. Song
School of Material Science and Engineering, Jiangsu University, Zhenjiang 212013, China
e-mail: shenxq@ujs.edu.cn
Fax: +86-0511-88791964

Y. Zhu
School of Mechanical and Electrical Engineering, Nanjing University of Aeronautics and Astronautics, Nanjing 210016, China

1 Introduction

The hexaferrites are ceramic magnetic materials and have played an important role in many technological and industrial fields. Among various hexaferrite materials, the *M*-type ferrite with a magnetoplumbite structure is widely used as high-density magnetic recording and microwave devices due to a low cost and an excellent magnetic property [1–3]. However, with the technology development, the pure *M*-type ferrite was hard to meet the requirements [4]. For high-density magnetic recording media, it is necessary to have a sufficiently high saturation magnetization and a low temperature coefficient of coercivity. In order to improve the magnetic properties of the pure *M*-type ferrites, various substitutions were investigated based on the fact that their structure and magnetic properties are closely related to the chemical composition and the arrangement of ions in the crystal unit [5]. Single and complex ion substitutions such as La [6], La–Cu [7], Ti–Zn [8], Sn–Ni [9], La–Zn [10, 11] and so on, were studied to tune the magnetic parameters. Bai et al. [4] and Liu et al. [10] prepared the La–Zn substituted strontium ferrite nanoparticles and films and found out a proper amount of La–Zn substituted could significantly improve the saturation magnetization and decrease the temperature coefficient of coercivity.

Recently, one-dimensional (1D) magnetic nanostructured materials have been investigated intensively due to their novel chemical and physical properties and their potential as building blocks for future electromagnetic devices

[12, 13]. To obtain 1D magnetic nanostructured materials, a lot of methods have been developed. As compared to other processes [14], the electrospinning technique has been proved to be a simple and versatile process for manufacturing 1D structural materials [15, 16]. A variety of materials, such as polymers [17], metal [18], metal oxides [16], and hybrid (organic/inorganic) nanofibers [19] have been prepared using the electrospinning method. In previous work, we prepared the pure strontium ferrite nanofibers [20]. The present work reported preparation of the La–Zn substituted strontium ferrite nanofibers using sol–gel assisted electrospinning, the effect of La–Zn ions substitution on the microstructure, morphology and magnetic properties of the resultant $Sr_{1-x}La_xZn_xFe_{12-x}O_{19}$ ($0.0 \le x \le 0.5$) nanofibers.

2 Experimental

The preparation of $Sr_{1-x}La_xZn_xFe_{12-x}O_{19}$ ($0.0 \le x \le 0.5$) nanofibers was similar to the process described in our previous paper [20] and consisted of solution preparation, electrospinning and calcination. In a typical procedure, 0.5 g poly(vinylpyrrolidone) (PVP, $Mw = 1{,}300{,}000$, Aldrich) was dissolved in a mixture of ethanol (4.5 g) and distilled water (2.0 g), followed by magnetic stirring for 2 h to ensure the dissolution of PVP. Then appropriate amount of strontium nitrate ($Sr(NO_3)_2$, AR), lanthanum nitrate ($La(NO_3)_3 \cdot 6H_2O$, AR), zinc acetate [$(Zn(CH_3COO)_2 \cdot 2H_2O)$, AR], and ferric nitrate [$(Fe(NO_3)_3 \cdot 9H_2O)$, AR] were added into the PVP–ethanol–water solution and further magnetically stirred for about 20–24 h at room temperature to form a homogeneous viscous solution for electrospinning. The viscous solution was loaded into a plastic syringe with a stainless steel needle. The needle used as the positive electrode was connected to a high-voltage supply and the solution was fed at a rate of 0.5 mL/h using a syringe pump during the electrospinning process. A piece of aluminum foil used as the ground collector was placed in front of the needle tip to collect the composite fibers. The distance between syringe needle tip and collector was 13 cm and the applied voltage was 15 kV. The as-spun $Sr_{1-x}La_xZn_xFe_{12-x}O_{19}$/PVP composite nanofibers collected were dried and calcined at 900°C for 2 h in ambient atmosphere to obtain the resultant nanofibers.

The X-ray diffraction (XRD) patterns were collected on a Rigaku $D/\max$ 2500PC diffractometer with Cu Kα radiation. Field emission scanning electron microscopy (FE-SEM, JSM-7001F) equipped with an Oxford INCA energy-dispersive X-ray (EDX) spectrometer were employed to analyze the morphology, chemical composition and microstructure of the samples. The magnetic properties of the as-prepared nanofibers were investigated at room temperature using a vibrating sample magnetometer (VSM, HH-15).

3 Results and discussion

3.1 Ferrite formation

Figure 1 shows the XRD patterns of $Sr_{0.8}La_{0.2}Zn_{0.2}Fe_{11.8}O_{19}$ nanofibers calcined at different temperatures for 2 h. After calcined at 600°C (Fig. 1a), the XRD collections are basically indexed to γ-Fe_2O_3 (JCPDS No. 39-1346) and $SrCO_3$ (JCPDS No. 05-0418). At this temperature, almost no crystalline zinc oxide and lanthanum oxide are detected; the reasons for this are that the content for these oxides is too low to be detected and these oxides may exist as an amorphous material. With the calcination temperature at 800°C (Fig. 1b), most of the peaks are assigned to the M-type strontium ferrite (JCPDS No. 33-1340). Meanwhile, $SrCO_3$ should be decomposed to SrO and CO_2, and γ-Fe_2O_3 is partially transformed into α-Fe_2O_3 (JCPDS No. 33-0664), which would react with other oxides to form the ferrite at a high calcination temperature [21]. When the calcination temperature increased up to 900°C (Fig. 1c), the single phase M-type ferrite is formed, which indicates that Zn^{2+} and La^{3+} ions enter the magnetoplumbite lattice. Then, the corresponding peaks for M-type ferrite become sharper and narrower with increasing calcination temperatures from 900 to 1000°C, implying crystallization improvement and grain growth.

Figure 2 shows the XRD patterns of $Sr_{1-x}La_xZn_xFe_{12-x}O_{19}$ nanofibers with various substitution contents calcined at 900°C for 2 h. With the substituted-ions content (x) increasing from 0 to 0.5, the peaks for M-type ferrite gradually become broaden, which means that the crystallization is restrained and the grain size becomes smaller.

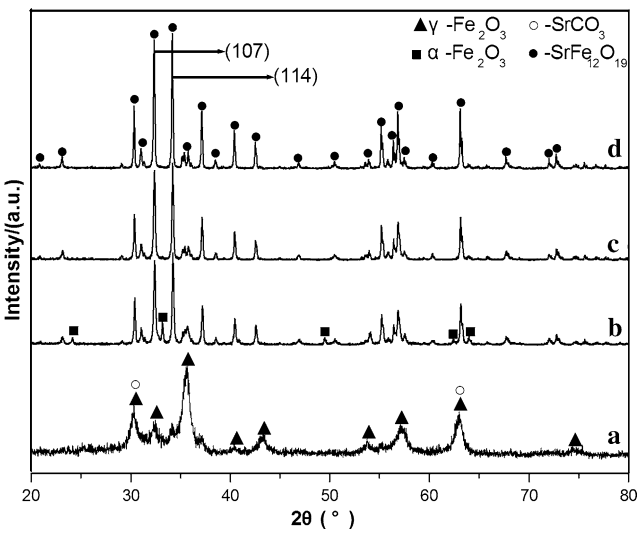

Fig. 1 XRD patterns of $Sr_{0.8}La_{0.2}Zn_{0.2}Fe_{11.8}O_{19}$/PVP composite nanofibers calcined at different temperatures: (**a**) 600°C; (**b**) 800°C; (**c**) 900°C; (**d**) 1000°C

Figure 3 shows the dependence of the lattice constants on the substituted-ions content (x) for La–Zn. It can be seen that both the lattice constants (***a*** and ***c***) decrease with the increase of x because the La^{3+} ion radius (1.22 Å) is smaller than the Sr^{2+} ion (1.27 Å) and the Zn^{2+} ion (0.83 Å) smaller than the Fe^{3+} ion (0.87 Å), respectively [4]. The lattice constant decrease with the La–Zn ions content indicates that the substitutions are accomplished. Consequently, the lattice constant variation would change the distance between magnetic ions in the unit cell. This will influence the exchange interaction and affect the magnetic properties of the strontium ferrite.

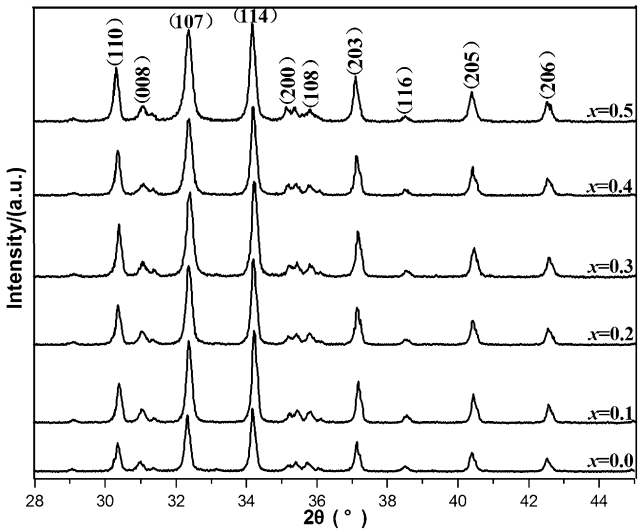

Fig. 2 XRD patterns of $Sr_{1-x}La_xZn_xFe_{12-x}O_{19}$ nanofibers calcined at 900°C for 2 h with different La–Zn substitutions (x)

The crystalline grain size of the strontium ferrite nanofibers can be calculated from the full-width at half-maximum (FWHM) of the XRD reflection (107) and (114) planes as showed in Fig. 1 using the Debye–Scherrer formula. The calculated D values for $Sr_{0.8}La_{0.2}Zn_{0.2}Fe_{11.8}O_{19}$ nanofibers calcined at the temperature from 800 to 1000°C are in the nanoscale ranging from 40 to 48 nm largely due to the mass transfer enhancement at a high temperature.

By referring the reflection (107) and (114) planes in Fig. 2, the calculated grain size of strontium ferrite with different substitution contents are represented in Fig. 4. From Fig. 4, it can be seen that with x increased from 0 to 0.5, the grain size reduces from 50 to 40 nm. It is well known that additives such as SiO_2, Al_2O_3, etc. are usually used to suppress the hexaferrite grain growth process due to grain boundary existences for these oxides [22]. For the ions substitution, the grain suppression mechanism should be different from the boundary effect resulting from the oxides of SiO_2, Al_2O_3, etc. As the substituted-ions of La–Zn in the lattice reduce the unit cell volume, these smaller unit cells would decrease the mass transportation among neighboring particles during the crystal growth and lead to smaller grains. Similar phenomena for the strontium ferrite powders and films were observed by Chen et al. [6] and Liu et al. [10], respectively.

3.2 Nanofiber morphology

The SEM morphologies of $Sr_{0.8}La_{0.2}Zn_{0.2}Fe_{11.8}O_{19}$ nanofibers calcined at different temperatures for 2 h are showed in Fig. 5. After calcined at 800°C, the nanofibers (Fig. 5a) are largely fabricated of nanoparticles about 80 nm with a plate-like morphology, and some smaller spherical particles

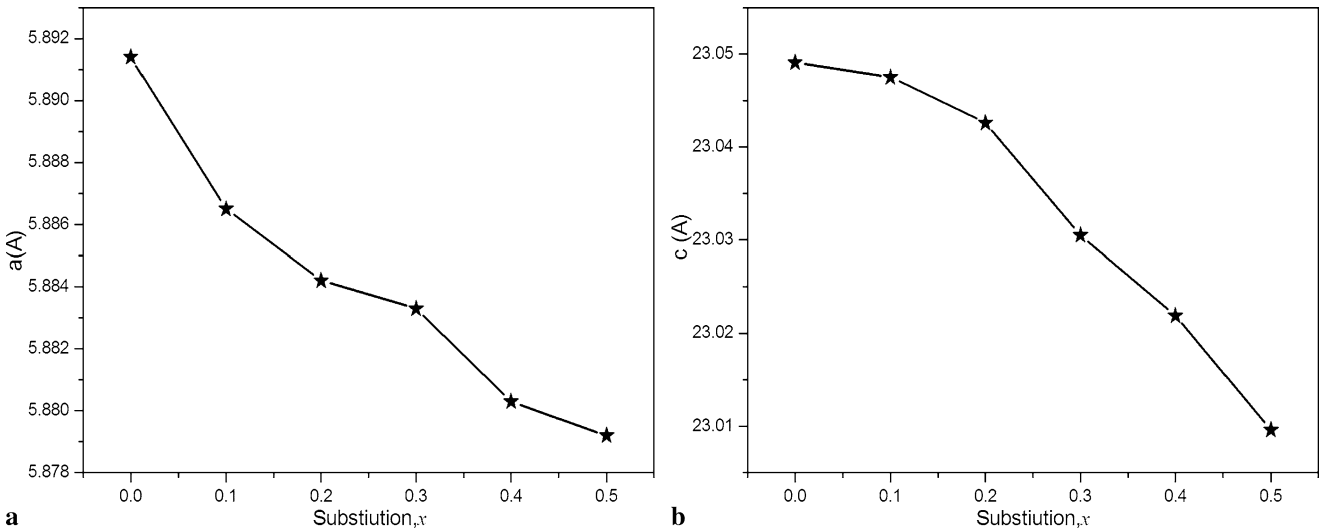

Fig. 3 Dependence of lattice constants ***a*** (**a**), and ***c*** (**b**) on different La–Zn substitution (x)

on the nanofiber surface, believed to be α-Fe_2O_3 as evidenced by the previous XRD analysis. With increasing calcination temperature from 800 to 1000°C, particle growth takes place and some very large particles occur by coalescence. It is interesting to note that the particle morphology tends to be elongated plate-like and the nanofibers possess a necklace-like structure connecting by these single elongated plate-like particles obtained at 1000°C as showed in Fig. 5c–d. This phenomenon is similar to the finding for the pure *M*-type strontium ferrite nanofibers [20] and it means that a low level of substituted ions of La–Zn almost has no obvious effects on the particle morphology.

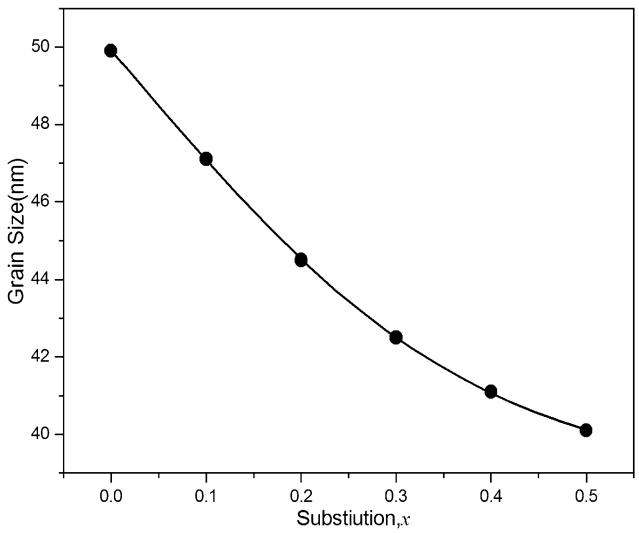

Fig. 4 Grain size of $Sr_{1-x}La_xZn_xFe_{12-x}O_{19}$ nanofibers calcined at 900°C for 2 h with different La–Zn substitutions (x)

The morphologies of $Sr_{1-x}La_xZn_xFe_{12-x}O_{19}$ ($0.0 \leq x \leq 0.5$) nanofibers with a uniform diameter about 100 nm obtained at 900°C for 2 h are showed in Fig. 6. With x increasing from 0 to 0.5, the particle morphology basically maintains the elongated plate-like structure except the particle size changed from a large size about 100 nm (Fig. 6a) to a small size about 60 nm (Fig. 6f), while the nanofiber morphology varies from the necklace-like structure (Fig. 6a–d) connecting by the elongated plate-like particles to the structure (Fig. 6e–f) building of multi-particles with a smaller size on the nanofiber cross-section. The nanofiber microstructure thus can be modified by design of the chemical composition and heat treatment.

In order to confirm the chemical composition of as-prepared $Sr_{1-x}La_xZn_xFe_{12-x}O_{19}$ nanofibers, a quantitative elemental analysis on these samples was carried out by the energy-dispersive X-ray spectrometer attached to the scanning electron microscope. Figure 7 shows the EDX spectra of the $Sr_{1-x}La_xZn_xFe_{12-x}O_{19}$ nanofibers, and the corresponding elemental analysis results are presented in Table 1. The results indicate that the atomic percentage (at %) of Sr, La, Zn, and Fe in the $Sr_{1-x}La_xZn_xFe_{12-x}O_{19}$ nanofibers determined by EDX basically agree with the designed composition.

3.3 Magnetic properties

Figure 8 shows hysteresis loops of the randomly oriented $Sr_{0.8}La_{0.2}Zn_{0.2}Fe_{11.8}O_{19}$ nanofibers obtained at different calcination temperatures for 2 h. It can be observed that the hysteresis loop for nanofibers calcined at 600°C has an intrinsic soft magnetic characteristic, with a specific saturation magnetization (Ms) of 34 A m^2 kg^{-1} and a coercivity

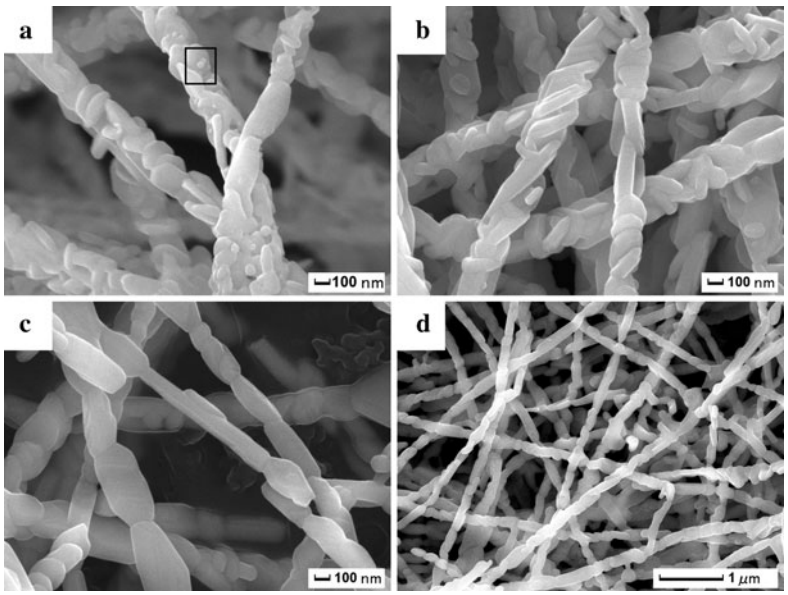

Fig. 5 SEM morphologies of $Sr_{0.8}La_{0.2}Zn_{0.2}Fe_{11.8}O_{19}$ nanofibers obtained at different calcination temperatures: (**a**) 800°C; (**b**) 900°C; (**c**) and (**d**) 1000°C

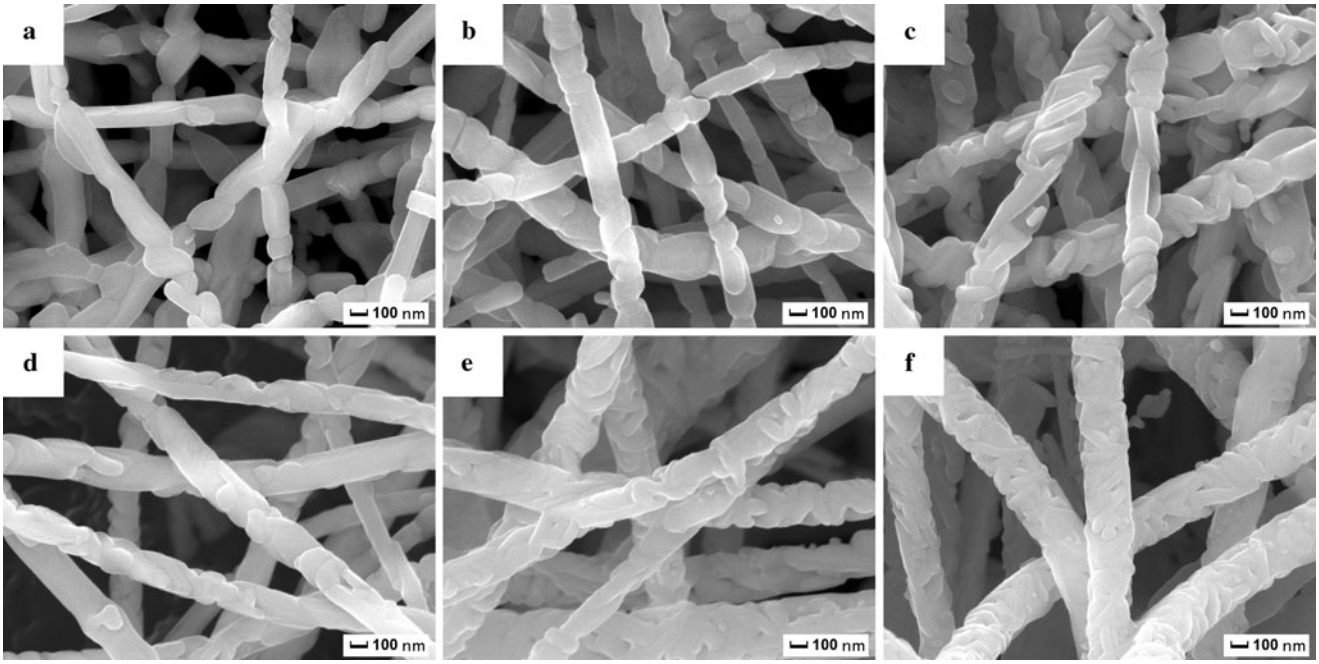

Fig. 6 SEM morphologies of $Sr_{1-x}La_xZn_xFe_{12-x}O_{19}$ nanofibers calcined at 900°C for 2 h with different La–Zn substitutions (x): (**a**) 0; (**b**) 0.1; (**c**) 0.2; (**d**) 0.3; (**e**) 0.4; (**f**) 0.5

Table 1 EDX elemental analysis results of $Sr_{1-x}La_xZn_xFe_{12-x}O_{19}$ nanofibers with different La–Zn substitutions (x)

x in $Sr_{1-x}La_xZn_xFe_{12-x}O_{19}$	Elemental compositions (at %)			
	Sr	La	Zn	Fe
0	3.0	–	–	37.3
0.1	2.7	0.3	0.3	35.0
0.2	2.6	0.6	0.7	37.1
0.3	2.2	1.0	1.1	35.6
0.4	1.9	1.3	1.3	36.4
0.5	1.6	1.7	1.6	35.7

(Hc) of 7 kA m^{-1} largely due to γ-Fe_2O_3 phase as proved in the previous Sect. 3.1. When calcined at the temperature of 800°C and higher the nanofibers exhibit a typical hard magnetic characteristic due to the M-type strontium ferrite formation. The Ms and Hc values estimated are relatively low when the nanofibers are calcined at 800°C because of the very small amount of α-Fe_2O_3 in the nanofibers. When calcined at 900°C the nanofibers achieve a maximum Ms value about 72 A m^2 kg^{-1}, and then almost maintain the Ms value around 71 A m^2 kg^{-1} with a further increase of calcination temperature to 1000°C. The Hc variation is different from the Ms value and shows a continuous increase from 252 to 354 kA m^{-1} corresponding to the calcination temperature from 800 to 1000°C. These phenomena can be explained by the Stoner–Wohlfarth single-domain theory [23] because the grain sizes (40–48 nm) of the $Sr_{0.8}La_{0.2}Zn_{0.2}Fe_{11.8}O_{19}$ nanofibers are lower than the M-type strontium ferrite single-domain critical size, about 60 nm [24, 25].

According to the Stoner–Wohlfarth single-domain theory, the magnetocrystalline anisotropy energy (E_A) of a nanocrystal single-domain is approximated by

$$E_A = KV\sin^2\theta$$

where K is an anisotropy constant, V is the volume of nanocrystal, and θ is the angle between the easy axis and direction of field-induced magnetization. Hc is closely related to E_A and is related to the grain size. The Hc value increase is mainly caused by the grain growth of the $Sr_{0.8}La_{0.2}Zn_{0.2}Fe_{11.8}O_{19}$ nanofibers with the calcination temperature increased.

The effect of substituted-ions content of La–Zn on Hc and Ms values for the randomly oriented $Sr_{1-x}La_xZn_xFe_{12-x}O_{19}$ nanofibers calcined at 900°C for 2 h are represented in Fig. 9. It can be seen from Fig. 9 that the coercivity at room temperature for the nanofibers shows a continuous reduction with increasing La–Zn ions substitution, from 413 ($x = 0.0$) to 219 kA m^{-1} ($x = 0.5$). This coercivity reduction can primarily be attributed to two major factors. First, the grain size of the $Sr_{1-x}La_xZn_xFe_{12-x}O_{19}$ nanofibers is reduced by the La–Zn substitution and the effect of grain size on Hc for the $Sr_{1-x}La_xZn_xFe_{12-x}O_{19}$ nanofibers is represented in Fig. 10. Second, we have the replacement of Fe^{3+} ions by the diamagnetism Zn^{2+} ions;

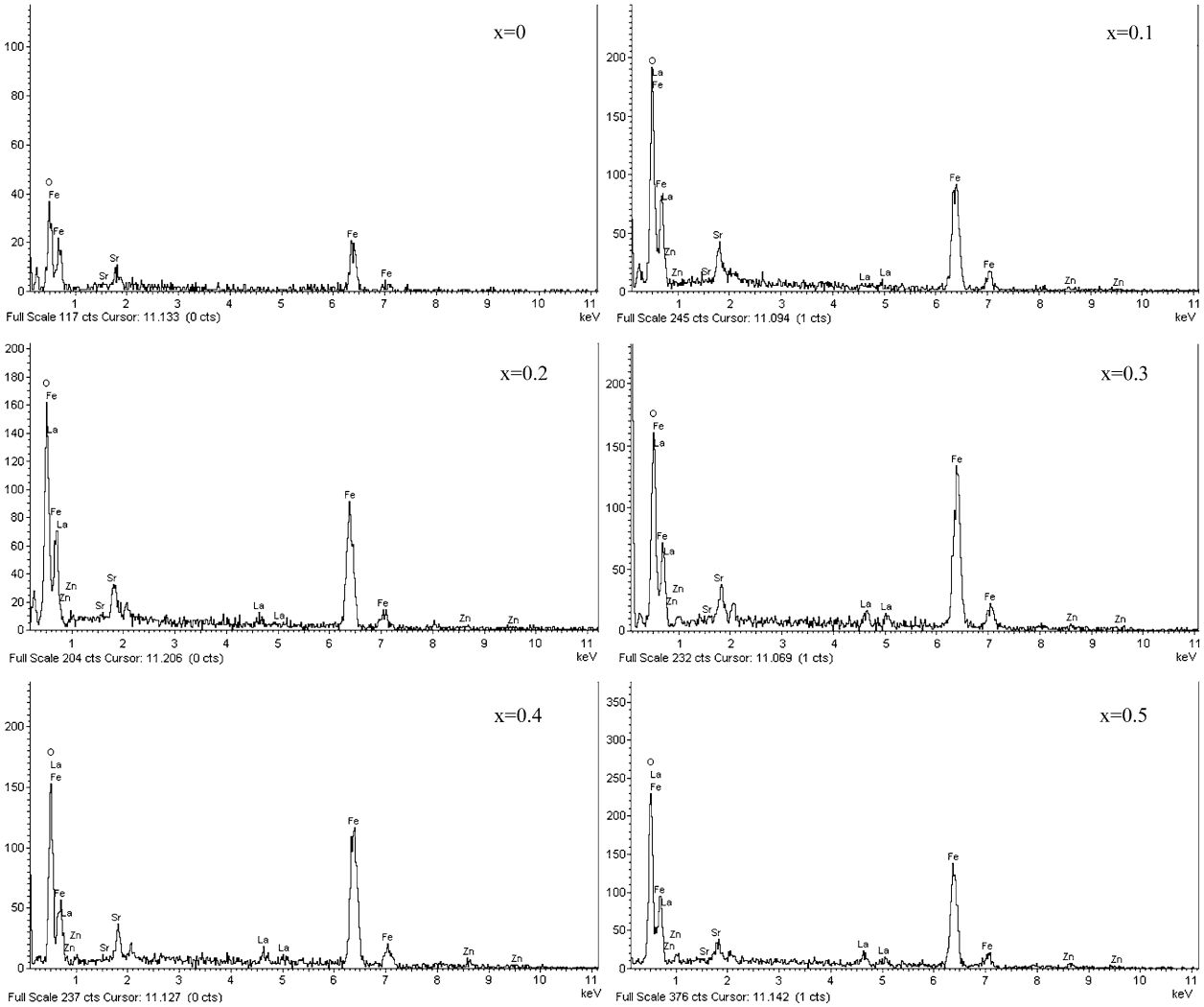

Fig. 7 EDX spectra of $Sr_{1-x}La_xZn_xFe_{12-x}O_{19}$ nanofibers with different La–Zn substitutions (x)

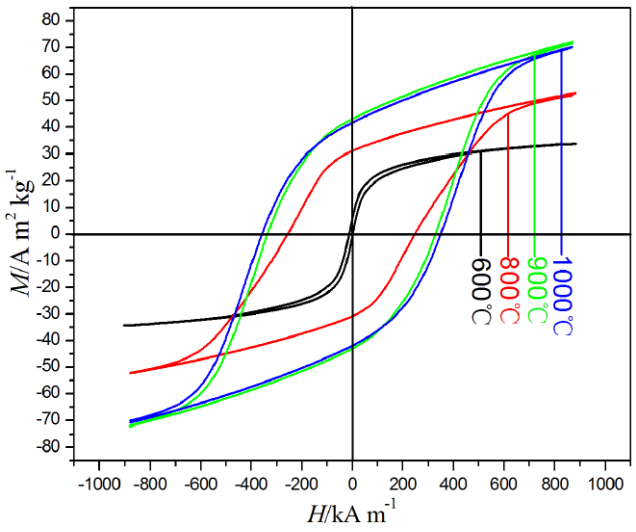

Fig. 8 Hysteresis loops of $Sr_{0.8}La_{0.2}Zn_{0.2}Fe_{11.8}O_{19}$ nanofibers obtained at different calcination temperatures

it causes the anisotropy constant to decrease [11]. For *Ms*, however, its value initially increases, reaching a maximum value of about 72 A m^2 kg^{-1} at $x = 0.2$, and then decreases with the substituted La–Zn content. A similar trend of the variation of magnetization with La–Zn ions substitution was reported for the hexaferrite powders and films [10, 11].

It is well known that in a unit cell of *M*-type ferrite, there are five distinct crystallographic sites or sublattices for the cations, three octahedral ($2a$, $12k$, $4f_2$), one tetrahedral ($4f_1$) and one trigonal bipyramid ($2b$). The spin directions for $2a$, $12k$ and $2b$ sublattices are parallel to each other (in the direction of the crystallographic c-axis), whereas those of the $4f_1$ and $4f_2$ sublattices are in the opposite direction, which are coupled by superexchange interactions through O^{2-} ions. The variation of *Ms* with the substituted-ion content of La–Zn can be explained on the basis of the exchange interaction between the Fe^{3+} ions at the different sites. According to the Mössbauer spectroscopy results re-

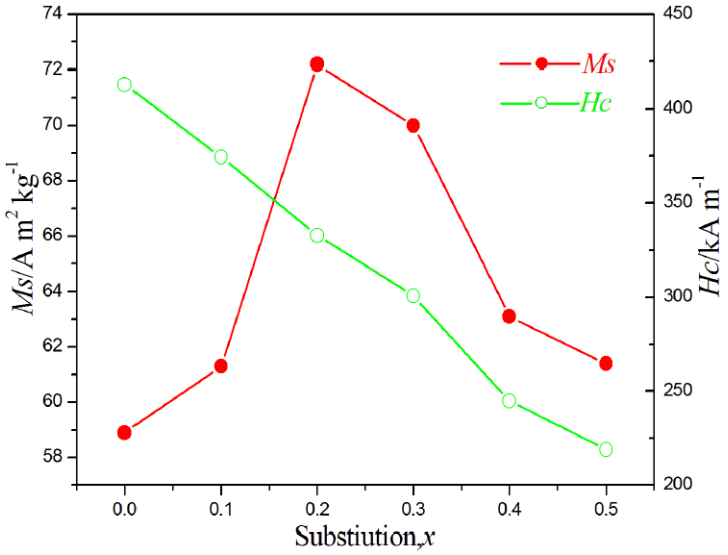

Fig. 9 Specific saturation magnetization (*Ms*) and coercivity (*Hc*) for $Sr_{1-x}La_xZn_xFe_{12-x}O_{19}$ nanofibers with La–Zn substitutions (x)

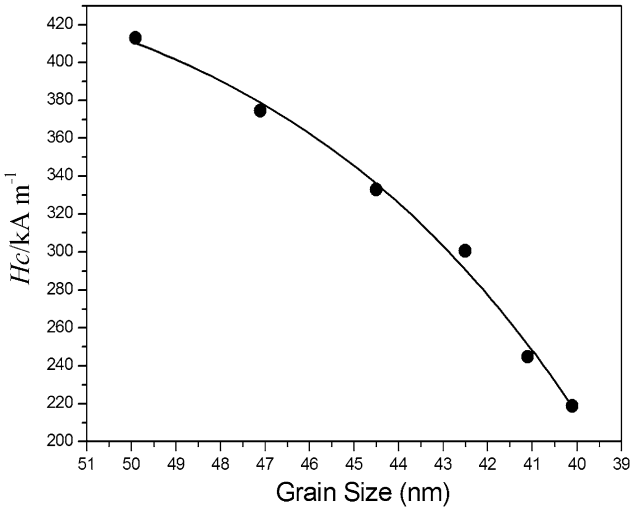

Fig. 10 Effect of grain size on coercivity (*Hc*) for $Sr_{1-x}La_xZn_xFe_{12-x}O_{19}$ nanofibers

ported in [26], the Zn^{2+} ions preferentially substitute the Fe^{3+} ions in the spin-down $4f_1$ site. This occupation will cause an increasing number of Fe^{3+} ions in spin-up sites compared to the number in spin-down sites, and as a result, an increase of *Ms* with x initially. For the pure strontium ferrite the magnetic moments of Fe^{3+} ions are commonly arranged collinearly due to the existence of superexchange interactions. However, as the La–Zn ions enter the lattice, the lattice constants decrease (as showed in Fig. 2), which will modify the magnetic ions arrangement in the unit cell and the exchange interaction. In particular, at a high level of La–Zn substitution, the modified exchange interaction will cause the collinear arrangement to the non-collinear arrangement for the magnetic moments of Fe^{3+} ions with the canting spin structure formation [4]. Thus, when the substituted La–Zn ions content (x) gets over 0.2, with the canting spin structure occurring in the unit cell, the *Ms* values will decrease with x increasing [4].

4 Conclusions

(1) The $Sr_{1-x}La_xZn_xFe_{12-x}O_{19}$ ($0.0 \leq x \leq 0.5$) nanofibers with diameters around 100 nm have been prepared by the sol–gel assisted electrospinning and calcination process with the metal salts and poly (vinylpyrrolidone) as starting regents.

(2) The grain size and morphology of the $Sr_{1-x}La_xZn_xFe_{12-x}O_{19}$ nanofibers are mainly influenced by the calcination temperature and substitution contents. With the substituted-ions content of La–Zn increased, the grain size decreases significantly, from about 50 nm ($x = 0.0$) to 40 nm ($x = 0.5$).

(3) The specific saturation magnetization (*Ms*) of the $Sr_{1-x}La_xZn_xFe_{12-x}O_{19}$ nanofibers is related to the substituted-ions content of La–Zn. When the $Sr_{1-x}La_xZn_xFe_{12-x}O_{19}$ nanofibers were calcined at 900°C for 2 h with $x = 0.2$ one can get a maximum *Ms* about 72 A m^2 kg^{-1}, higher about 13 A m^2 kg^{-1} than that for the pure strontium ferrite nanofibers. The coercivity for the nanofibers shows a continuous reduction with increasing La–Zn ions substitution, from 413 ($x = 0.0$) to 219 kA m^{-1} ($x = 0.5$) owing to the grain size decease due to the La–Zn substitution and the anisotropy constant reduction arising from the replacement of Fe^{3+} ions by the diamagnetism Zn^{2+} ions.

Acknowledgements This work was financially supported by the National Natural Science Foundation of China (Grant No. 50474038), Research Fund for the Doctoral Program of Higher Education of China

(Grant No. 20103227110006), Aviation Science Foundation (Grant No. 2009ZF52063) and the Jiangsu Provincial Postgraduate Cultivation and Innovation Project (Grant No. CX10B-257Z).

References

1. B.S. Zlatkov, M.V. Nikolic, O. Aleksic, H. Danninger, E. Halwax, J. Magn. Magn. Mater. **321**, 330 (2009)
2. S.P. Castaneda, J.R. Martńez, F. Ruiz, S. Palomares-Sánchez, J.A. Matutes-Aquino, J. Magn. Magn. Mater. **250**, 160 (2002)
3. J. Dho, E.K. Lee, J.Y. Park, N.H. Hur, J. Magn. Magn. Mater. **285**, 164 (2005)
4. J.M. Bai, X.X. Liu, T. Xie, F.L. Wei, Z. Yang, Mater. Sci. Eng. B **68**, 182 (2000)
5. D.H. Choi, S.W. Lee, I.B. Shim, C.S. Kim, J. Magn. Magn. Mater. **304**, e243 (2006)
6. N. Chen, K. Yang, M.Y. Gu, J. Alloys Compd. **490**, 609 (2010)
7. L. Qiao, L.S. You, J.W. Zheng, L.Q. Jiang, J.W. Sheng, J. Magn. Magn. Mater. **318**, 74 (2007)
8. C.S. Wang, F.L. Wei, M. Lu, D.H. Han, Z. Yang, J. Magn. Magn. Mater. **183**, 241 (1998)
9. D. Lisjak, M. Drofenik, J. Eur. Ceram. **24**, 1841 (2004)
10. X.X. Liu, J.M. Bai, F.L. Wei, H. Xu, Z. Yang, J. Appl. Phys. **87**, 2503 (2000)
11. J.C. Corral-Huacuz, G. Mendoza-Suárez, J. Magn. Magn. Mater. **242–245**, 430 (2002)
12. S.K. Nataraj, B.H. Kim, M.D. Crue, Mater. Lett. **63**, 218 (2009)
13. L. Luo, B.D. Sosnowchik, L.W. Lin, Appl. Phys. Lett. **90**, 093101 (2007)
14. Y. Xia, P. Yang, Y. Sun, Y.Y. Wu, B. Mayers, B. Gates, Y.D. Yin, F.L. Kim, H.Q. Yan, Adv. Mater. **15**, 353 (2003)
15. D. Li, J.T. McCann, Y.N. Xia, M. Marquez, J. Am. Ceram. Soc. **89**, 1861 (2006)
16. A. Greiner, J.H. Wendorff, Chem. Int. Ed. **46**, 5670 (2007)
17. J.D. Schiffman, C.L. Schauer, Polym. Rev. **48**, 317 (2008)
18. J.L. Shui, J.C.M. Li, Nano Lett. **9**, 1307 (2009)
19. X. Lu, C. Wang, Y. Wei, Small **5**, 2349 (2009)
20. X.Q. Shen, M.Q. Liu, F.Z. Song, X.F. Meng, J. Sol-Gel Sci. Technol. **53**, 448 (2010)
21. P. Veverka, K. Knížek, E. Pollert, J. Boháček, S. Vasseur, E. Duguet, J. Portier, J. Magn. Magn. Mater. **309**, 106 (2007)
22. X.H. He, Q.Q. Zhang, Z.Y. Ling, Mater. Lett. **57**, 3031 (2003)
23. E.C. Stoner, E.P. Wohlfarth, IEEE Trans. Magn. **27**, 3475 (1991)
24. C.S. Lin, C.C. Huang, T.H. Huang, G.P. Wang, C.H. Peng, Mater. Sci. Eng. B **139**, 24 (2007)
25. R. Nawathey-Dikshit, S.R. Shinde, S.B. Ogale, S.D. Kulkarni, S.R. Sainkar, S.K. Date, Appl. Phys. Lett. **68**, 3491 (1996)
26. S.W. Lee, S.Y. An, I.B. Shim, C.S. Kim, J. Magn. Magn. Mater. **290–291**, 231 (2005)